Effect of Annealing on Thermal and Dynamic Mechanical Properties of Poly(lactic acid)

Assia Zennaki
Université Aboubakr Belkaïd
Latifa Zair
Université Aboubakr Belkaïd
Khadidja Arabeche
Université Aboubakr Belkaïd
Lina Benkraled
Université Aboubakr Belkaïd
Ulrich Maschke (ulrich.maschke@univ-lille.fr)
UMET – Unité Matériaux et Transformations, UMR 8207, Univ. Lille, CNRS, INRAE, Centrale Lille
Abdelkader Berrayah
Université Aboubakr Belkaïd

Research Article

Keywords: Poly(lactic acid), thermal properties, mechanical properties, annealing, crystallization, phase transition.

Posted Date: June 23rd, 2022

DOI: https://doi.org/10.21203/rs.3.rs-1758641/v1

Effect of Annealing on Thermal and Dynamic Mechanical Properties of Poly(lactic acid)

Assia Zennaki[a], Latifa Zair[a], Khadidja Arabeche[a], Lina Benkraled[a], Ulrich Maschke[b,*], Abdelkader Berrayah[a]

A. Zennaki, Dr. L. Zair, Prof. K. Arabeche, L. Benkraled, Prof. A. Berrayah

Laboratoire de Recherche sur les Macromolécules, Faculté des Sciences, Université Aboubakr Belkaïd, 13000 Tlemcen, Algeria

Dr. U. Maschke

UMET – Unité Matériaux et Transformations, UMR 8207, Univ. Lille, CNRS, INRAE, Centrale Lille, F-59000 Lille, France

E-mail: ulrich.maschke@univ-lille.fr

ABSTRACT

Effects of annealing temperature (T_a: 80-140°C) and time (t_a: 3-30 h) on the crystalline phase transition in poly(lactic acid) (PLA) were studied by Differential Scanning Calorimetry (DSC) and Dynamic Mechanical Analysis (DMA). In the DSC curves, the sample annealed at T_a=80°C with time interval (t_a: 10-30 h) demonstrates a peculiarly small exothermal peak (T_{exo}) around 130°C, just prior to the melting point, corresponding to the disorder-to-order (α'-to- α) phase transition, while the sample annealed at temperature (T_a: 90-110°C) shows a double melting behavior considered as the α'- α phase transition. At T_a>110°C, the α' -form of PLA was found to transform into the α one during the annealing process. The α'- α phase transition around 100°C (T_a: 90-110°C), determined from the two melting peaks (T_{m1} and T_{m2}) as function of T_a at different times t_a, shows a good correlation with the substantial increase in the crystallinity rate (X_c) with a maximum of 32% at T_a=120°C. Towards low temperatures, the glass modulus E_g reported by DMA thermograms, shows an important increase (~30 000 MPa) at T_a=80°C for t_a=3 h, due to the nucleation density extremely high in low PLA materials crystallization. After a sharp drop to 3 600 MPa at T_a=110°C, a marked improvement of E_g (15 900 MPa) is observed around T_a=120°C for all samples, regardless of time t_a, temperature region where PLA is usually molded in the industrial melt processing. This interesting effect (improvement of E_g in range T_a=100-120°C) can be correlated with the grow of crystallinity in the same domain of T_a, and the α'- α phase transition T_a (T_a: 90-110 °C) determinate by the double T_m melting DSC peak, which is confirmed by the increase of T_g for T_a=90-110°C.

Keywords: Poly(lactic acid); thermal properties; mechanical properties; annealing; crystallization; phase transition.

Introduction

Poly (lactic acid) (PLA) is a biodegradable plastic, derived from renewable resources; it is a material of choice [1-7] in applications of various domains such as biomedicine, food packaging, textile, electronics, etc. PLA is characterized by slow crystallization kinetics often observed in conventional processing methods (extrusion, injection, etc.). This phenomenon is highly problematic, with significant consequences on thermal and mechanical properties of the final product. In many applications, increasing the crystallinity of PLA is desired because, in its amorphous form, the field of application of PLA is severely limited by its low glass transition temperature (T_g). At temperatures higher than T_g, only the crystalline phase of PLA can impart valuable mechanical properties. Thus, the crystalline form is necessary to increase the strength of the material [8-11]. Annealing is widely used for the recrystallization of PLA-based materials [12-15]. Improvement of thermo-mechanical properties is sometimes obtained by mixing PLAs of different molar masses or with other biodegradable polymers [16, 17].

Typically, PLA homopolymer has three crystal forms [18-22], such as α-, β-, and γ-form, which depend on the crystallization conditions. Among all these crystal forms, the α-form is the most common and stable polymorph. It has been shown that PLA is polymorphic [23-28], exhibiting two different crystalline phases termed α and α'. Crystallization of the relaxed melt at temperatures above 120°C leads to the formation of α -crystals with a 10_3 helical chain conformation where two chains are interacting in an orthorhombic unit cell [18, 29, 30]. At temperatures lower than 100°C only α'-crystals develop. In the α'-form, the molecule segments adopt the same helical structure as in α-crystals, however they exhibit conformational disorders [30]. Within the 100-120°C crystallization temperature range, a mixture of crystalline phases α' and α was present. The α'-crystals are metastable at their formation temperature but transform into the stable α-form upon heating at their stability limit of around 150°C [23-25, 30-34]. Zhang and coauthors [31, 32] confirmed

that the small exothermic peak T_{exo} in the DSC curve, detected just prior to the melting peak, is associated with the disorder-to-order (α'to α) phase transition. This exothermic signal, already reported by Ohtani et al. [35], Chao et al. [36] and Zhao et al. [37], has been confirmed by Zhang and coauthors [31, 32] by DSC, WAXD, and IR techniques. In the DSC thermograms, two endothermic peaks appear, related to the melting of the α' and α phases. The peak at the lower temperature is related to the melting of the α' -form and its recrystallization into the α form, while the second peak corresponds to the melting of the α -form. The two processes, the melting of the α' form and the recrystallization into the α form, can be considered as the α'-α phase transition.

This study aims to understand the fundamental effect of annealing time t_a and temperature T_a on the thermal and mechanical behavior of PLA. The α'- α phase diagram as function of t_a and T_a was determined by melting peaks from DSC data. Crystallinity of annealed PLA as a function of T_a for different t_a will be determined and correlated with the α'-α phase diagram. Through the DMA data, the glass modulus E_g and loss tangent $tan\delta$ of annealed PLA, as a function of T_a for different t_a, was determined and analyzed for particular conditions of T_a and t_a. Correlation between α'-α phase transition and crystallinity, mechanical properties (E_g) and molar mass (M_v) will be discussed.

Material and Methods

Materials

The poly(lactic acid), supplied by NatureWorks (USA), was a semi-crystalline 4043D grade material comprising around 4% mol of D-isomer units. The PLA pellets were transparent and amorphous.

Sample Preparation

PLA granules were dried in a vacuum oven at 50°C for 24h, then melted at 200°C and compressed into a sheet with a thickness of about 1 mm. The melted-compressed PLA sheet was immediately quenched into ice water to obtain an amorphous PLA sheet. Amorphous PLA is then annealed in a vacuum oven, at temperatures T_a: between 80°C and 140°C, and time t_a between 3h and 30 h. In the present study, the PLA samples of un-annealed (amorphous) and annealed at different T_a and t_a are referred to as "un-aPLA" and "aPLA" (T_a; t_a); for example, aPLA (T_a=80°C; t_a=30h) means annealed sheet at 80°C and 30h.

Molecular Weight Measurement

The molecular weight of PLA was determined from its intrinsic viscosity [η] measurement applying the Mark-Houwink equation, using an Ubbelohde-type capillary viscometer at 25°C. Chloroform was used as solvent. The viscosity average molecular weight M_v was calculated from the intrinsic viscosity by using the following equation [38]:

$$[\eta] = 5.45 \times 10^{-4} {M_v}^{0.73} \quad (1)$$

Thermal Analysis

DSC measurements were performed on a TA Q2000 DSC apparatus equipped with a Refrigerated Cooling System (RCS90) allowing cooling down to -90°C. Temperature and heat flow scales were calibrated with high purity indium standards. Hermetic aluminum pans (Tzero, TA Instruments) were used, which are able to stand an internal pressure of 300 kPa. Samples of about 10 mg were analyzed under nitrogen gas flow at a heating rate of 10°C/min from 25°C to 200°C, kept at the latter temperature for 2 min; cooled back to 25°C, followed by an isothermal scan for 2 min. The crystallinity rate (X_c) induced by the

thermal treatment could be deduced from the heat flow signal obtained by DSC, using the following equation [39]:

$$Xc = \frac{\Delta H_m - \Delta H_c}{\Delta H_c^0} \quad (2)$$

where ΔH_m and ΔH_C are the enthalpies of melting and crystallization of the PLA samples, respectively, and ΔH_c^0 represents the enthalpy of fusion of the PLA crystal of infinite size, which was reported by Fischer et al. [40] to be 93.1 (J/g).

Dynamic Mechanical Analysis

Dynamic mechanical analysis were performed using a DMA Q800 (TA, Inc.). Experiments were conducted in tensile mode at a frequency of 1 Hz. Curves displaying storage (*E*') and loss (*E*") moduli were recorded as a function of temperature between 25°C and 180°C applying a heating rate of 3°C/min. The amplitude and the preload force are 5 µm and 0.010 N, respectively. The shape of the PLA films was rectangular, with dimensions 10 × 6 × 1 mm^3. The temperatures of various relaxation processes were determined from the $tan\delta$ temperature curve at 1 Hz. The glass transition temperature (T_g) can be defined as the maximum of the transition in the loss tangent curve.

RESULTS AND DISCUSSION

DSC analysis

Fig. 1 illustrates a comparison of DSC thermograms of the as-received PLA-pellet dried in a vacuum oven at 50°C and the un-annealed sample (un-aPLA), taken as reference sample for all thermograms. un-aPLA exhibits amorphous behavior with a very low crystallinity rate (X_c=1.6%) and a glass transition at 60°C. An exothermic peak T_{cc} associated with a cold crystallization process appears at 127.2°C, following by an endotherm event with a

central peak at T_m=153.4°C. The results from thermal analysis of un-aPLA sample and PLA-pellets are given in Table 1.

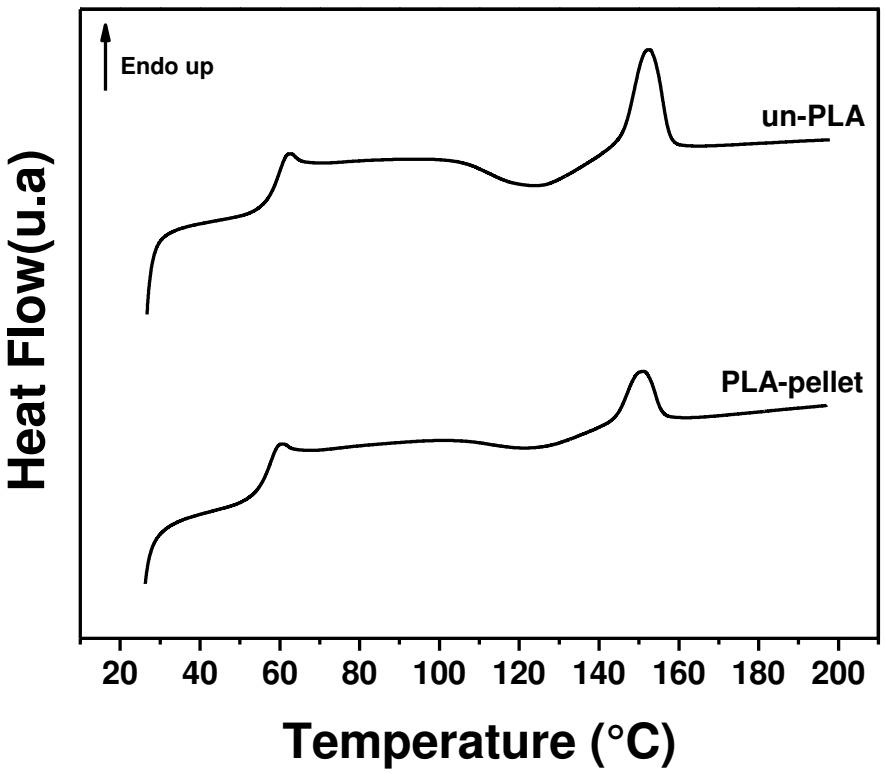

Fig. 1 DSC thermograms of as-received PLA-pellet and the un-aPLA sheet.

Table 1 Results from thermal analysis of PLA-pellets and un-aPLA sample.

Sample	T_g (°C)	T_{cc} (°C)	ΔH_c (Jg^{-1})	T_m (°C)	ΔH_m (Jg^{-1})	X_c (%)
PLA-pellets	59.5	125.8	1.65	152.5	3.60	2.1
un-aPLA	60.0	127.2	3.41	153.4	4.86	1.6

DSC curves of aPLA (T_a: 80-140°C; t_a: 3-30h) samples were analyzed. Annealing PLA samples at 80°C and times t_a: 3-30h were illustrated in Fig. 2. The small exothermal peak T_{exo}, just prior to the melting point, associated with the disordered-order α'-α phase transition, clearly appears for t_a=10-30h. This exothermal event, previously reported par

Zhang et al. [31], was found to be in agreement with reports from many authors [22-30].

Thermal properties of aPLA (T_a=80°C; t_a=3h) sample were given in Table 2.

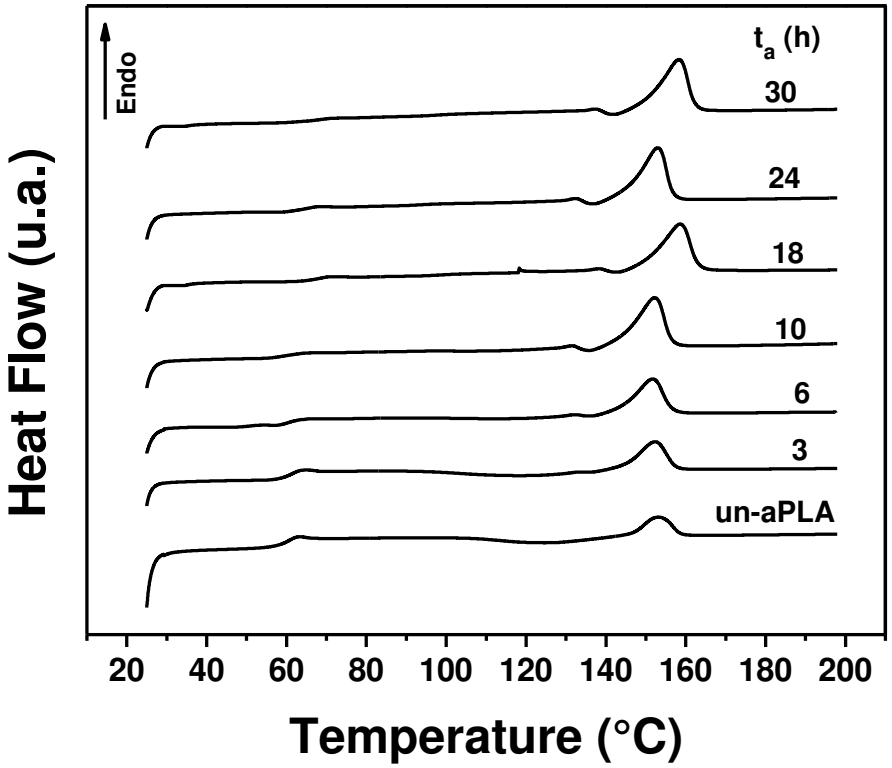

Fig. 2 DSC curves of aPLA sheets at T_a=80°C for times t_a = 3-30h.

Table 2 Results from thermal analysis of annealed samples at T_a=80°C for t_a = 3-30h.

Sample	t_a (h)	T_g (°C)	T_{cc} (°C)	ΔH_c (Jg^{-1})	T_{exo} (°C)	T_{m1} (°C)	T_{m2} (°C)	ΔH_m (Jg^{-1})	X_c (%)
	3	61.5	116.1	3.75	-	152.0	-	10.61	7.4
aPLA	6	62.1	118.0	0.85	-	153.1	-	13.81	13.9
(80°C-t_a)	10	60.2	-	-	131.8	152.4	-	16.78	18.0
	18	63.5	-	-	132.9	152.8	-	17.43	18.7
	24	65.6	-	-	132.3	152.6	-	17.83	19.2
	30	62.7	-	-	131.9	152.4	-	17.84	19.2

DSC curves of PLA annealed at 90 and 100°C were shown in Fig. 3. The small exothermal peak disappears, and an additional melting peak (T_{m2}) was observed in the form of a small shoulder (Fig. 3a) that stretches towards long annealing times in the case of aPLA (T_a=90°C; t_a: 3-30h). The two peaks, low-intensity T_{m2} (α' phase) and high-intensity T_{m1} (α phase), present a α'-α phase transition, with a α' phase in minority. In the case of annealing at 100°C (Fig. 3b), the two peaks (T_{m2} and T_{m1}) appear for all annealing times (t_a: 3-30 h), thus showing a α'-α transition of phases with the same order of magnitude. Results of thermal properties of aPLA (T_a=90, 100°C; t_a: 3-30 h) samples are given in Table S1.

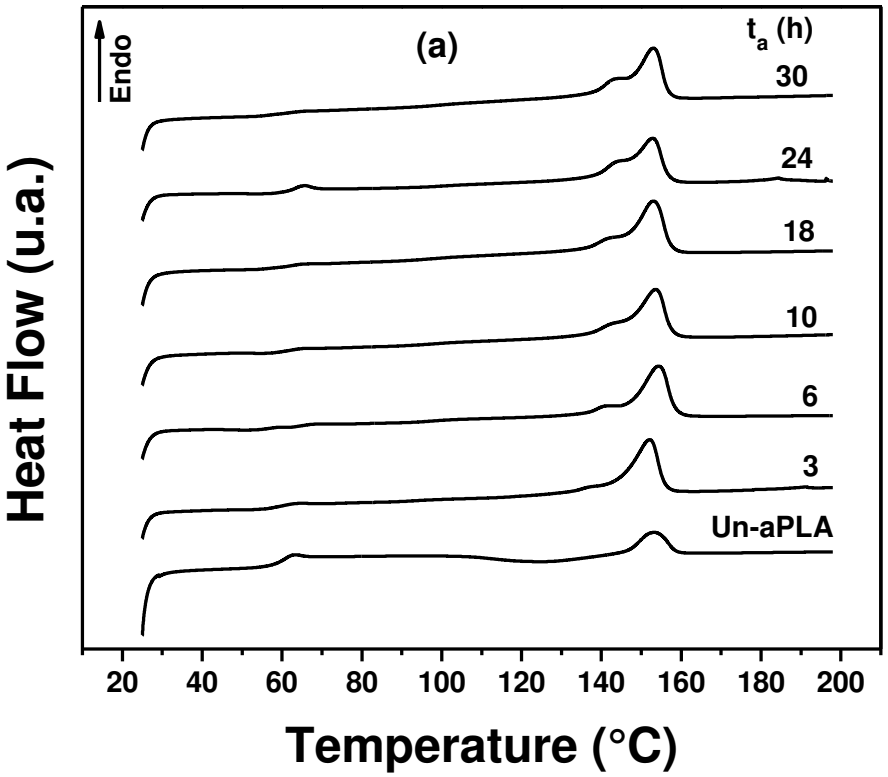

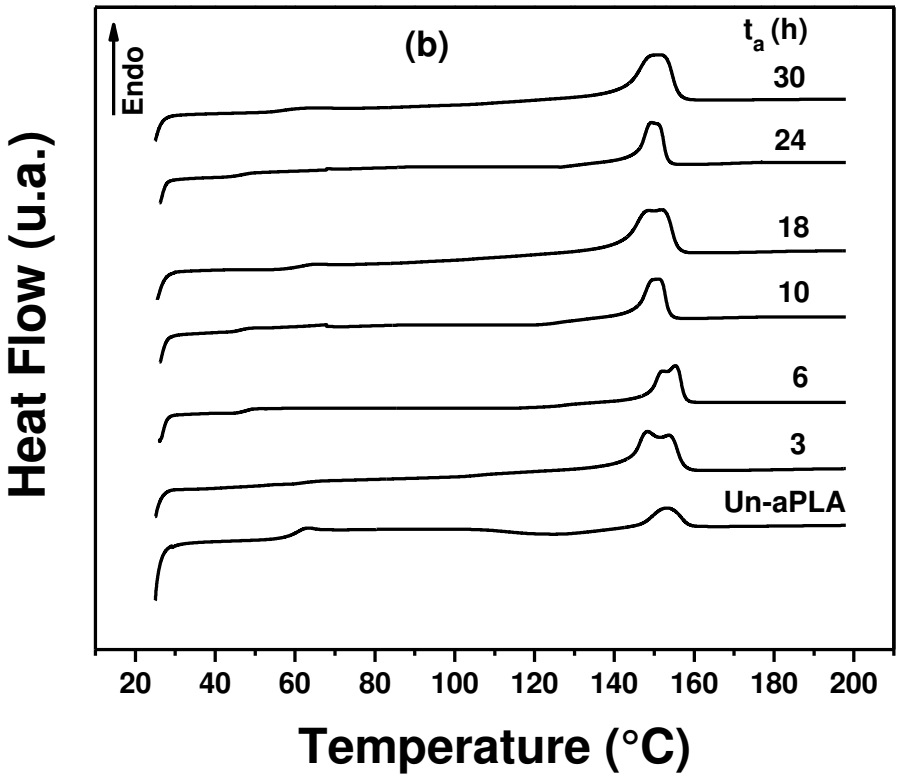

Fig. 3 DSC curves of aPLA samples for times t_a: 3-30h, at (a) T_a=90°C and (b) T_a=100°C.

Samples annealed at T_a=110°C for t_a=3 and 6 h show two peaks, T_{m2} of high intensity and T_{m1} as weak shoulder (Fig. 4), indicating the presence of a α'-α phase transition. Annealing for t_a=10h yields to a single high-intensity T_{m2} peak indicating that the α' phase is completely transformed into the α phase. Results from thermal analysis of aPLA (T_a=110°C; t_a: 3-30 h) are given in Table 3.

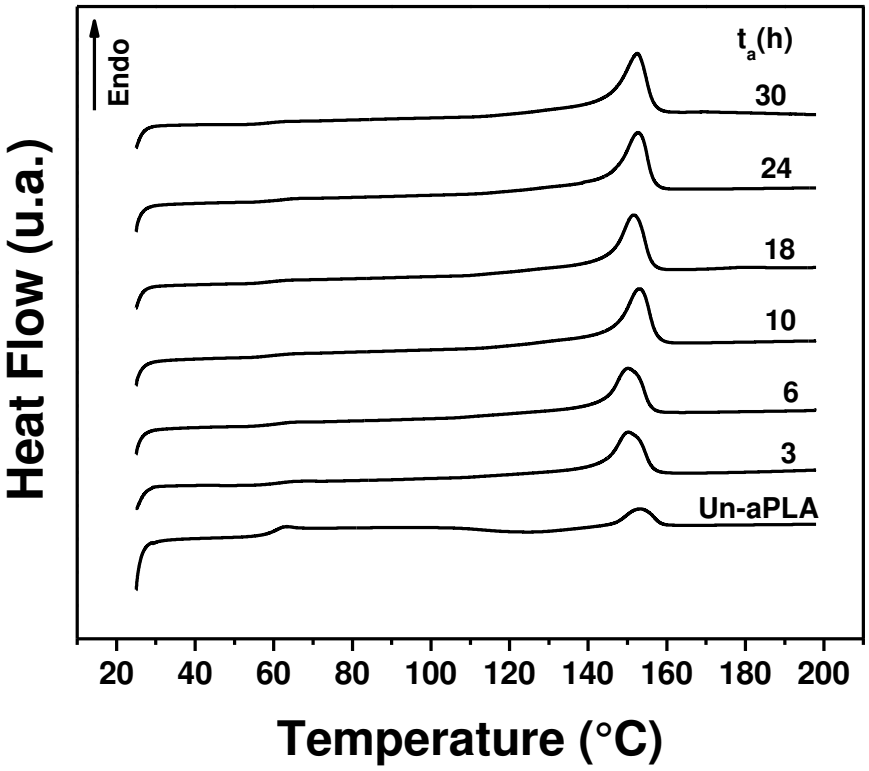

Fig. 4 DSC curves of aPLA samples at T_a=110°C for t_a: 3-30h.

Table 3 Thermal properties of annealed samples at 110°C for T_a=3-30h.

Sample	t_a (h)	T_g (°C)	T_{cc} (°C)	ΔH_c (Jg^{-1})	T_{exo} (°C)	T_{m1} (°C)	T_{m2} (°C)	ΔH_m (Jg^{-1})	X_c (%)
aPLA(110°C-t)	3	62.1	-	-	-	152.8	150.2	17.96	19.3
	6	62.1	-	-	-	151.6	150.1	19.17	20.6
	10	59	-	-	-	-	152.9	20.84	22.4
	18	59.3	-	-	-	-	151.5	21.17	22.7
	24	62.4	-	-	-	-	152.6	23.42	25.2
	30	59.4	-	-	-	-	152.4	23.67	25.4

Fig. 5 shows a single peak T_{m2} of high intensity when annealing at T_a=120°C, thus indicating that the α' phase is wholly transformed into the α phase. Beyond T_a=120°C, the

α phase is perfectly established, as shown in Fig. S1a and b, corresponding to the PLA samples annealed at 130 and 140°C. Results of the thermal properties of samples annealed at T_a=120, 130, and 140°C are given in Table S2.

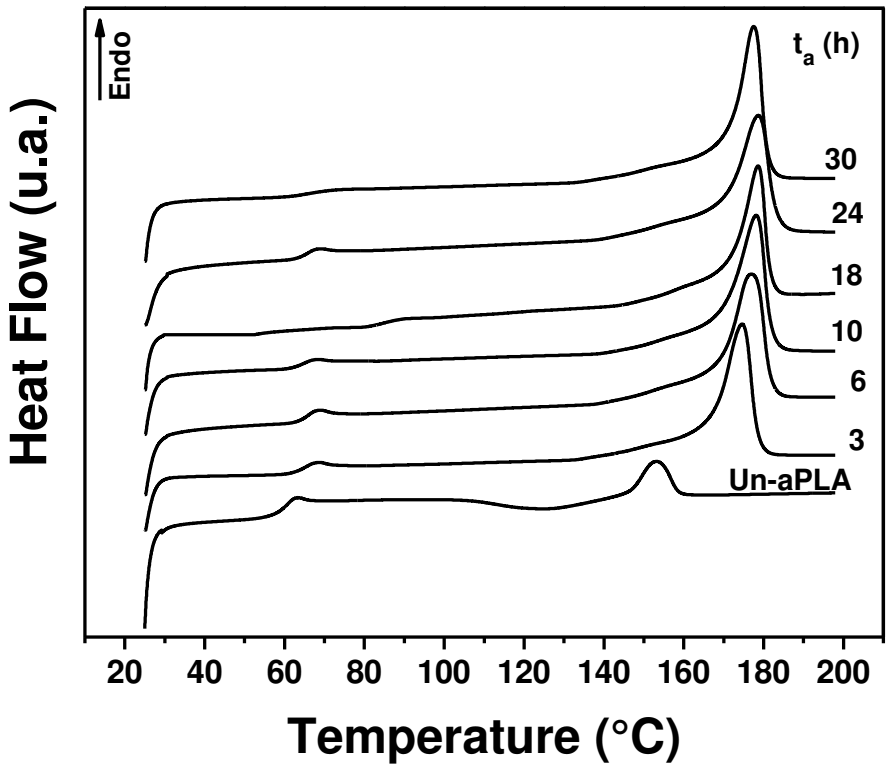

Fig. 5 DSC curves of aPLA samples at T_a=120°C for annealed times (t_a = 3-30 h).

α'-α phase diagram

The α'-α phase diagram, built from temperatures of T_{exo}, T_{m1} and T_{m2} peaks, is of great interest to better understand the evolution of the crystal structure as function of t_a and T_a. Fig. 6a gives a follow-up of α' and α as function of T_a for different t_a. The lower and upper limits of the α'-α *phase* transition require special attention. The lower limit of the α'-α transition coincides with the appearance of T_{m1} and T_{m2}; but often it is below 5 to 10°C since the α' -form transforms into α at T_{exo}. The upper limit is determined by linear extrapolation of T_{m2}, which is considered to correlate with the melting phenomenon of the

α-form. Giving the equilibrium melting temperature (T_m^0) at T_m=T_a, the Hoffman-Weeks equation can be written as [41] :

$$T_m = T_m^0\left[1 - \frac{1}{r}\right] + \frac{1}{r}T_a \quad (3)$$

where $1/r$ is the stability parameter which depends on the crystal thickness, and r represents the ratio of the lamellar thickness to the lamellar thickness of the critical nucleus at T_a. Fig. 6b shows the Hoffman-Weeks plots of aPLA, at 3h and 24h for different T_a, showing the upper limits towards T_a=110°C. The α'-α phase transition is therefore situated between 90°C and 110°C with $T_m^0 = 168.3$°C and 172.3 °C for aPLA at t_a=3h and 24h, respectively. Table 4 reports T_m^0 and $1/r$ for aPLA at different times (t_a: 3-24h).

Since α' crystals transform to α crystals upon heating, only annealing temperatures above T_a≥110°C were considered, where the α crystals are predominantly produced. It has been firmly established that crystallization at high supercooling of the melt, defined by $\Delta T = T_m^0 - T_a$, allows the development of increasingly smaller nuclei of supercritical size than crystallization at low supercooling. The aPLA (T_a=80°C; t_a=3h) sample clearly shows high supercooling ($\Delta T \approx 88$°C) compared to the aPLA (T_a=120°C; t_a=24h) sample which presents low supercooling (ΔT≈52°C). The aPLA (T_a=80°C; t_a=3h) sample with high supercooling develops increasingly smaller nuclei of supercritical size.

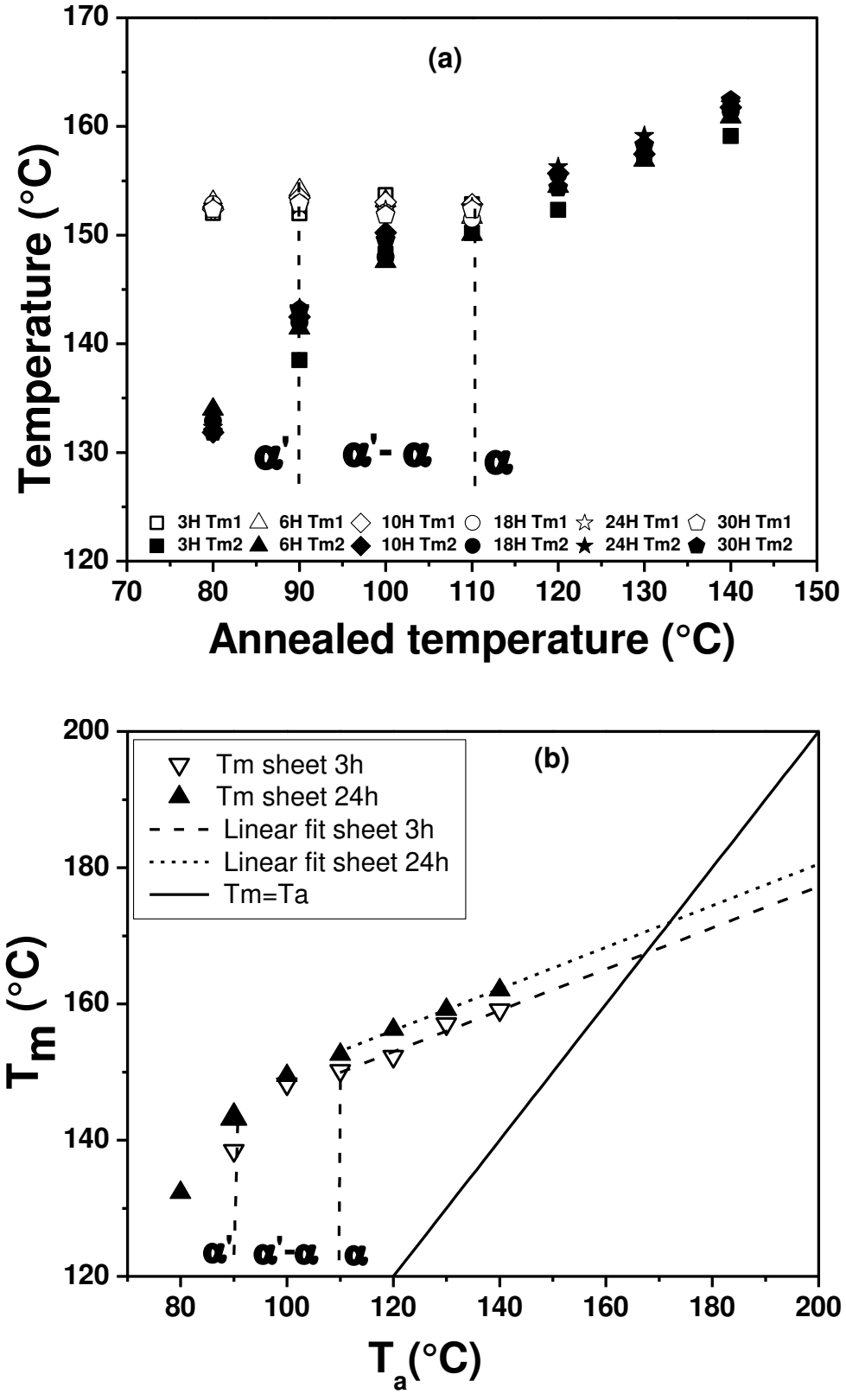

Fig. 6 (a) Melting peaks T_{m1} and T_{m2} plotted as a function of T_a for t_a: 3-30 h; (b) Hoffman-Weeks plots for aPLA for 3h and 24h at different temperatures.

Table 4 Equilibrium melting temperature T_m^0 and stability parameter ($1/r$) for aPLA at different times.

Samples	t_a (h)	T_m^0 °C	$1/r$	R^2
Hoffman-Weeks plots for annealed PLA for 3h-24h	3	168.3	0.314	0.96
	6	171.9	0.348	0.98
	10	169.7	0.284	0.96
	18	170.9	0.315	0.97
	24	172.3	0.312	0.99

The domain of the α'-α phase transition is often reported in the literature between 100°C and 120°C [27, 31-33], which is highly desirable for molding and extrusion to get optimal crystallinity. However, this domain is sometimes shifted towards lower or higher temperatures, strongly depending on heat treatment, molecular weight, external induced effects, etc. Jalali et al. [27] observed the domain of the α'-α phase transition between 100°C and 120°C for PLA samples, exhibiting the highest crystallization temperature, the highest nuclei density, and the smallest spherulite size. Zhang et al. [31, 32] showed that for PLA of molecular weight M_w=150 000 g/mol, the α'-α phase transition is located at 110°C< T_c< 130°C while for low molecular weights (M_w=50 000 g/mol), it was found around 105-130°C. Kawai et al. [33] showed that from melt-crystallization at T_c=80°C, the peak T_{exo}, characterizing the α' phase, appears clearly for different heating rates from 1 to 20°C/min, and that the range of the α'-α phase transition can be estimated to be around 80-120°C. Pan et al. [25] found that the α'-α transition depends entirely on t_a (0-24h) and T_a (120-160°C), and M_w affects the crystalline phase transition significantly, which can be explained by the mobility of polymer chains. Zhou et al. [42] studied deformational behavior and structural evolution of amorphous and aPLA samples stretched within 100-150°C. The amorphous PLA stretched at 120°C exhibits excellent mechanical properties.

The aPLA (T_a; t_a) sample, considered in this study, presents a α'-α phase transition around 90-110°C, as shown in Fig. 6a, i.e. slightly shifted towards lower temperatures, compared to the standard range 100-120°C.

Effect of annealing temperature and time on crystallinity

Fig. 7 shows the effect of T_a for different times t_a on the crystallinity rate X_c, evaluated using Eq. 1. At T_a=80°C, samples annealed during 3h and 6h exhibit X_c=7.4% and 14.8% with a cold crystallinity at 116°C and 117°C, respectively. This is in good agreement with the work of Mijovic´ et al. [43], Tsuji et al. [44] and Park et al. [45] where grainlike morphology was observed during cold crystallization at 80°C. Annealing times of 3h and 6h are not sufficient to achieve complete crystallinity which occurs at times t_a=10-30h around X_c=19%. For annealing temperatures in the range 80°C≤T_a<90°C at t_a: 10-30h, the cold crystallinity disappears, and X_c show plateau values around 19% (Fig. 7), which can be explained by the presence of the disordered α' phase (see thermograms of Fig. 2). For annealing temperatures in the range 90°C≤T_a<110°C, the crystallinity begins to increase at 90°C with more substantial growth from 100°C up to 110°C (X_c≈25% for T_a=110°C at t_a=24 h). For T_a>110°C, X_c grows to reach an optimal crystallinity (X_c≈32%) at 120°C. The domain of α'-α phase transition (90°C≤T_a<110°C), reported by the melting peaks T_m (Fig. 6a), is shifted by approximately 10°C towards lower temperatures compared to that predicted by X_c vs. T_a. In the latter case, above 110°C, X_c increases rapidly to an optimal value of 32% followed by a plateau above 120°C. On the other hand, the first case clearly shows a α'-α phase separation, with the presence of the two melting peaks limited to 110°C. The strong growth of X_c at T_a>110°C is due to discontinuities and strong growth of the dimensions of the spherulites observed in the same temperature range, as already mentioned by several authors [43-47]. Mijovic´ et al. [43] showed a series of optical micrographs taken at different times during melt- and cold-crystallization at 140°C and

80°C, respectively. The resulting morphologies are quite different; larger and more perfect spherulites were formed during melt-crystallization at 140°C whereas a grainlike morphology was observed during cold crystallization at 80°C. Tsuji et al. [44] found that the radii of spherulites of melt-crystallized PLLA samples increased dramatically from 10 μm to 150 μm when the annealing temperature (T_a) was increased from 100°C to 160°C. Park et al. [45] observed that density and size of spherulites increase with an increase of annealing time and temperature. For a semi-crystalline polymer, crystal growth rate is generally faster when T_a is close to its crystallization temperature [45–47].

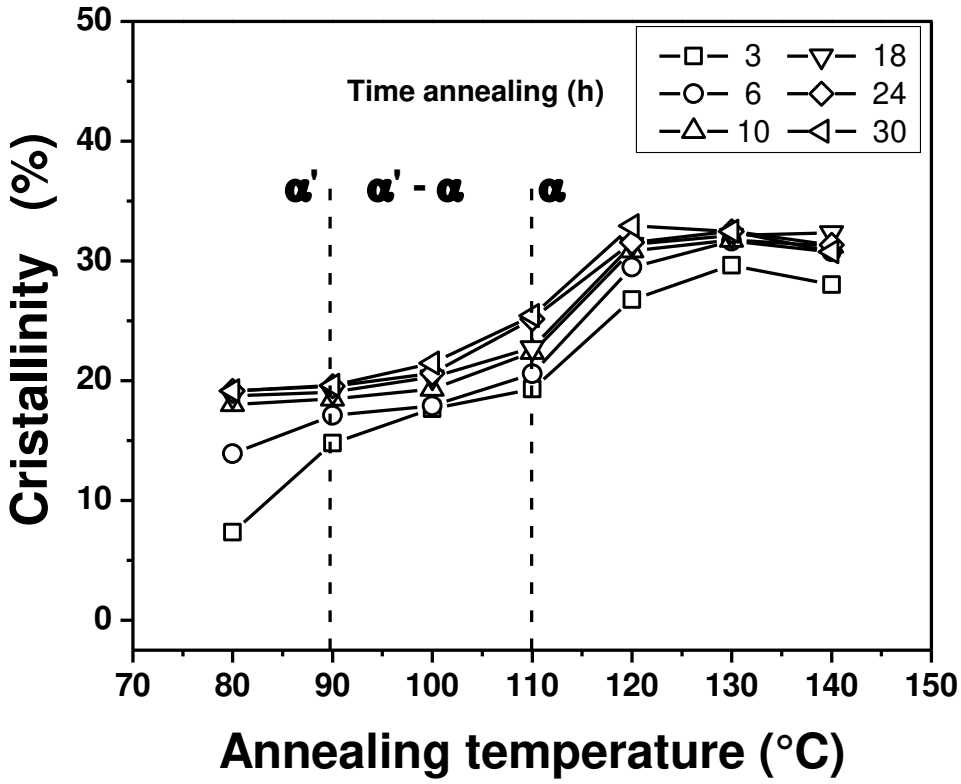

Fig. 7 Crystallinity of aPLA as a function of temperature T_a for different times t_a.

Dynamic mechanical behavior

Figs. 8 and 9 illustrate storage modulus E' and $tan\delta$ (defined as E''/E') of PLA sheet as function of temperature, for un-aPLA and aPLA (T_a: 80-140°C; t_a: 3-24h), respectively. The shape of E' thermograms (i.e., drop, rise and drop) of un-aPLA and aPLA (T_a=80°C;

t_a=3, 6h), is associated with the recrystallization process as given by Fig. 8a and b. Above T_g, the increase of the chain mobility favors the crystallization process, which proceeds due to a slow scan rate (3°C/min) coupled with sinusoidal solicitation.

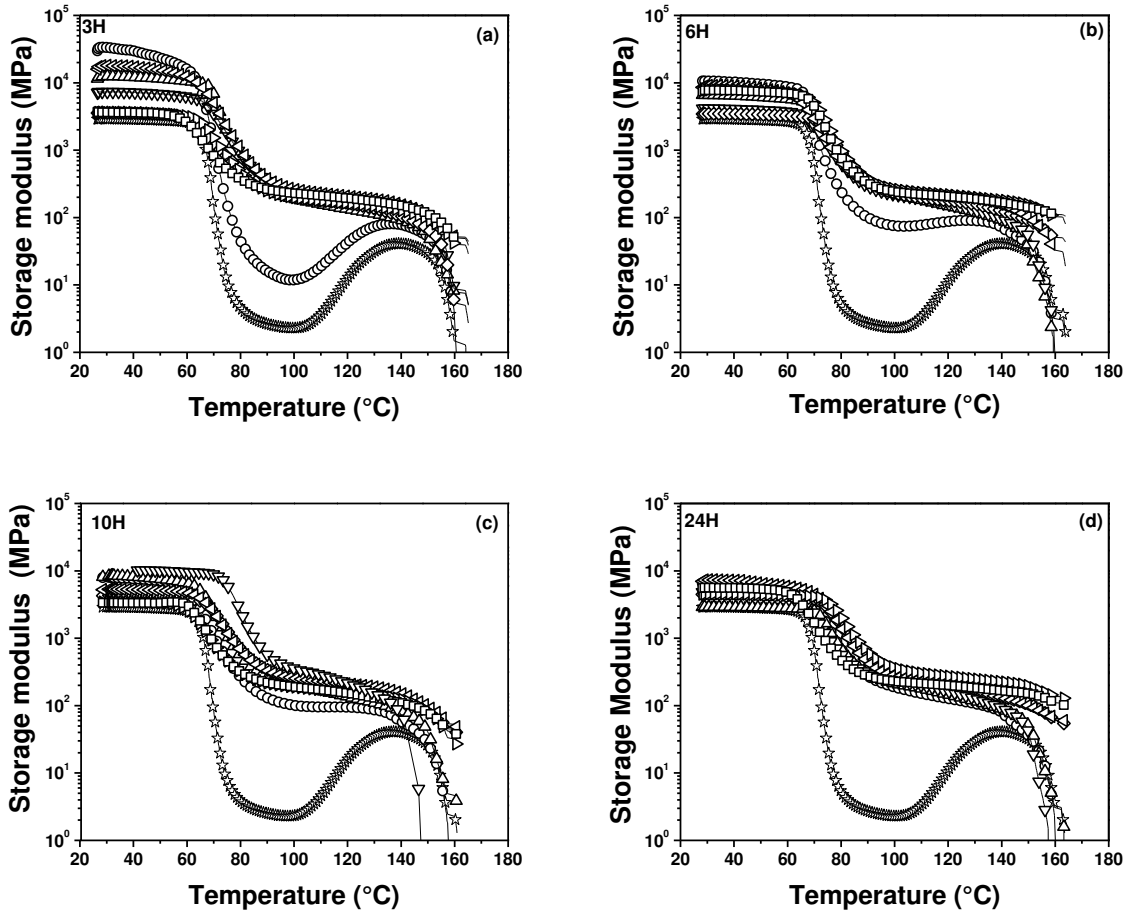

Fig. 8 Storage moduli of un-PLA and aPLA (T_a: 80-140°C; t_a) as a function of temperature for different annealing times. Symbols represent : ☆un-aPLA, O aPLA80, △ aPLA90, ▽ aPLA100, ◇ aPLA110, ◁ aPLA120 ▷ aPLA130, □ PLA140.

Incompletely crystallized, samples show around 100°C an increase in E' ($T>T_g$), caused by the cold crystallization phenomenon. The recrystallization induces stiffening of the macromolecular chains, responsible for the increase of the storage modulus. Towards high temperatures, the storage modulus drops when the material starts to flow, corresponding to

crystal melting of the material. The drop of E' values of un-aPLA and aPLA (T_a=80°C; t_a=3, 6h) samples is much faster than that in the case of highly crystallized aPLA (T_a: 90-140°C; t_a=3,6h) and aPLA (T_a: 80-140°C; t_a=10-24h) samples, which do not exhibit any further recrystallization process ($T>T_g$) and behave as perfectly semi-crystalline material. Thus, annealing, and therefore crystallization, can improve the heat resistance of PLA mainly due to restriction of molecular motion by the formation of firm spherulites.

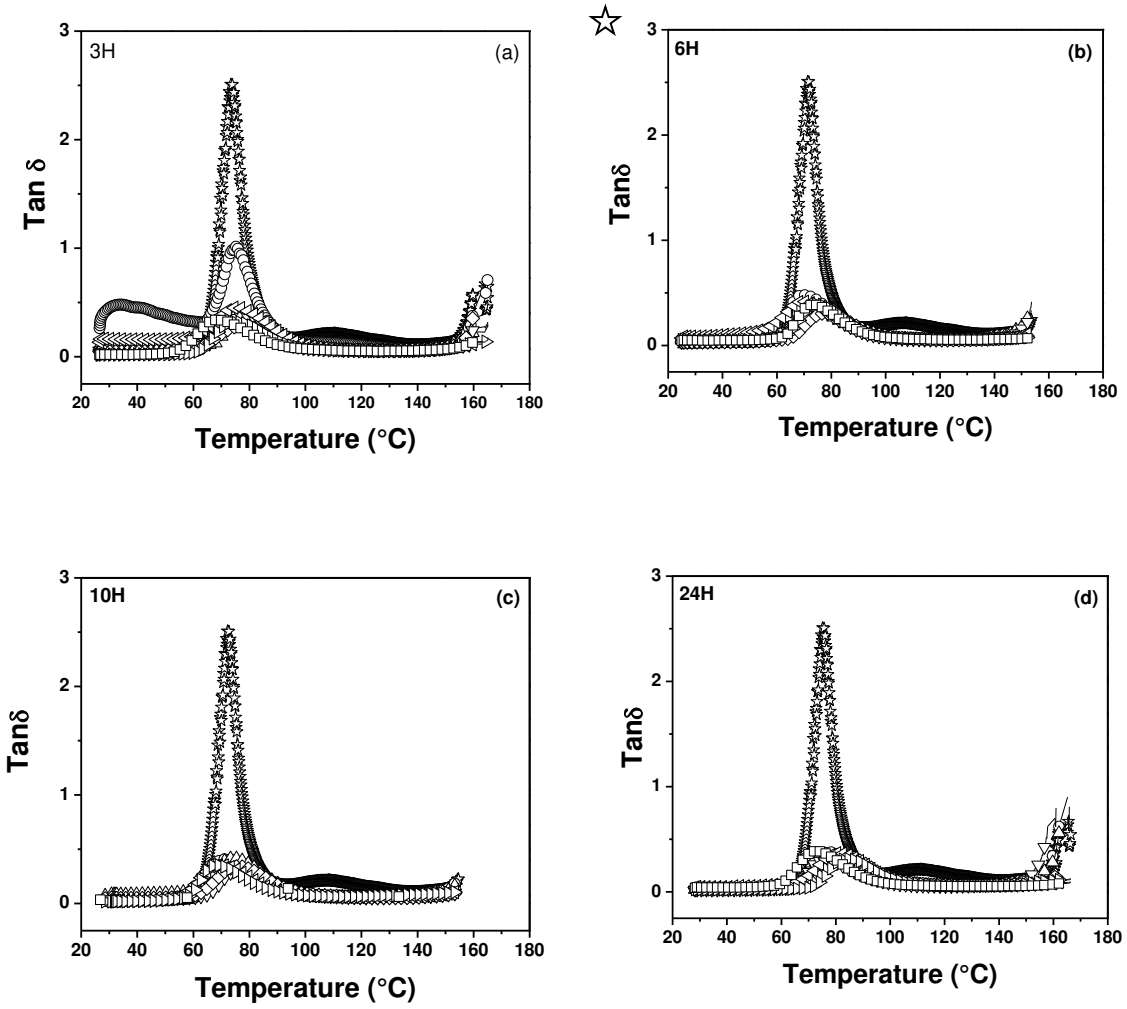

Fig. 9 *Tanδ* of un-PLA and aPLA (T_a: 80-140 °C; t_a) as a function of temperature for different annealing times. Symbols represent: ☆ un-aPLA, O aPLA80, △ aPLA90, ▽ aPLA100, ◇ aPLA110, ◁ aPLA120 ▷ aPLA130, □ PLA140.

The behavior of $tan\delta$ around T_g of un-aPLA and aPLA (T_a: 80-140°C; t_a: 3-24h) are presented in Fig. 9. The major relaxation process is associated with T_g, measured by the temperature of $tan\delta$ peak, where the sharpness and height are affected by the crystallinity. The un-aPLA sample behaves like an amorphous polymer showing a very sharp and intense $tan\delta$ peak because there is no restriction to the motion of the main chain. On the other hand, in semi-crystalline polymers, the dispersed crystalline regions hinder the chain mobility in the amorphous regions that is illustrated by a reduction of sharpness and height of the $tan\delta$ peak. A significant reduction of the height of the $tan\delta$ peak is observed for aPLA (T_a=80°C; t_a=3h) (Fig. 9a) with the same sharpness due to the low crystallinity (X_c=7.4%) and the presence of cold crystallinity. $tan\delta$ of aPLA (T_a: 90-140°C; t_a=3h) is represented by a sharp enlargement with a decrease of peaks due to the increase in crystallinity (16.5 to 32.1%), thus showing the semi-crystalline behavior of these samples. $tan\delta$ of aPLA (T_a: 80-140°C; t_a) samples annealed at 6h, 10h, and 24 h, shows wide peaks with low amplitudes, thus characterizing a perfectly semi-crystalline behavior as shown in Fig. 9b, c and d.

Effects of annealing temperature and time on PLA stiffness

The salient fact which emerges from thermograms of Figs. 8 and 9 is the behavior of glassy moduli E_g and loss $tan\delta$ as function of annealing temperature T_a at different times t_a, observed for low temperatures and around the glass transition. T_g's of different aPLA (T_a; t_a) samples, illustrated in Table 5, show an increase for T_a (T_a: 90-110°C) and t_a (t_a: 3-24 h), thus presenting greater rigidity to the material, particularly for the sample annealed at t_a=24 h with T_g=80.1°C. The increase of T_g in the range T_a: 90-110°C is due to the growth of crystallinity as shown in Fig. 7. This can be correlated with the α'-α phase transition domain (T_a: 90-110°C), given by DSC data in Figs. 6 and 7, thus confirming the improvement of the stiffness of the material [28, 31-33].

Table 5 DMA glass transition temperatures of aPLA (T_a: 80-140°C; t_a: 3-24 h). The T_g for un-aPLA corresponds to 75.2°C.

Annealing temperature (°C)	T_g - 3h (°C)	T_g - 6h (°C)	T_g - 10h (°C)	T_g - 24h (°C)
80	74.8	73.6	71.9	77.6
90	75.6	77.5	76.9	79.3
100	77.3	79.5	76.1	75.0
110	77.8	78.1	76.8	80.1
120	73.5	73.9	75.7	76.0
130	73.6	74.3	73.6	77.3
140	68.6	71.9	71.1	71.2

The stiffness of aPLA (T_a; t_a) samples can be also viewed through the typical glassy plateau E_g (Fig. 8), observed for all samples, depending on crystallinity and molecular weight. Given the same molecular weight, E_g should increase with crystallinity, but this trend was not observed. Indeed, PLA degrades due to thermal cleavage causing thus a substantial reduction of its molecular weight. This is an inevitable effect that must be taken into account when setting processing and annealing conditions of the material. Through monitoring E_g vs. T_a at different t_a (Fig. 10), two particular effects emerge from aPLA (T_a=80°C; t_a=3h) and aPLA (T_a=120°C; t_a): firstly, the very high value of E_g (29 900 MPa) of aPLA (T_a=80°C; t_a=3h), and secondly the improvement of E_g around T_a=120°C for all annealing times (t_a: 3-24h). This improvement can be represented by the reduced glassy modulus E_{gR} equal to the ratio of the maximum modulus (E_{gmax}) along the curve t_a and the maximum modulus ($E_{gmax120}$) at T_a=120°C (E_{gR}=E_{gmax}/$E_{gmax120}$). The sample annealed at t_a=24h presents the highest ratio (E_{gR}=0.9), corresponding to a strong crystallinity generated by the couple (T_a, t_a), which will be elucidated in the next chapter. After a drop from T_a=80°C, E_g begins to increase around T_a=100°C for all annealing times (t_a: 3-24h),

to reach a maximum value at T_a=120°C, corresponding to the maximum of crystallinity (Fig. 7).

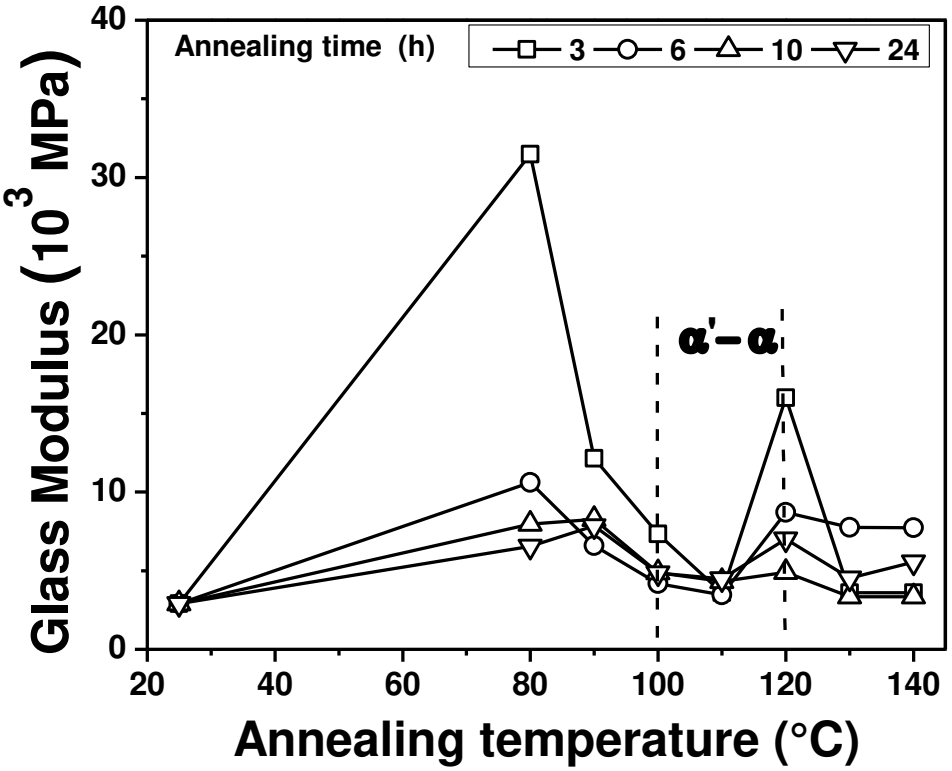

Fig. 10 Glass modulus E_g of annealed PLA as a function of T_a for t_a: 3-24 h. E_{gR} of the t_a curves is 0.5, 0.8, 0.8 and 0.9 relative to annealing times 3, 6, 10 and 24 h, respectively.

This improvement in rigidity around T_a=120°C, independently of t_a, corresponds to the (α'-α) phase separation, obtained from DSC data (Figs. 6 and 7). This can be explained by the fact that despite a high T_a (120°C), which is supposed to reduce the rigidity of the material thermally, an improvement of the modulus E_g is observed in the range T_a: 100-120°C. This effect, linked to the (α'-α) phase transition, is highly sought after in the molding and extrusion of PLA type materials.

Effects of crystallinity and molecular mass on aPLA (T_a=80°C; t_a) and aPLA (T_a; t_a=24h) samples

Crystallinity and molecular weight M_v directly influence the behavior of the glass modulus. If crystallinity tends to increase E_g, decrease of M_v, on the other hand, tends to make it fall. To better understand these relationships, E_g, X_c and M_v were determined as function of t_a and T_a, to analyze particular effects concerning aPLA (T_a=80°C; t_a=3h) and aPLA (T_a=120°C; t_a=24h) samples (Fig. 10). Concerning the first sample, E_g suddenly increases from the un-annealed state (2 900 MPa) up to 29 900 MPa at t_a=3 h despite the drop of M_v from 40 200 g/mol to 15 700 g/mol (Fig. 11a). Regarding crystallinity, the slight increase of X_c (~8%) cannot be the cause of this spectacular increase of the modulus. Indeed, structure and molecular mobility of the amorphous phase are strongly affected by the crystalline morphology developed in semi-crystalline polymers. The first indication comes from the theory of nucleation [48-56]. More particularly, a self-nucleation effect [49-53] could originate from smaller clusters or residual segmental orientation remaining in the melt, which play a role as precursors of the subsequent crystallization. From an industrial point of view, self-nucleation could be highly attractive to reduce time needed to process polymeric materials and to improve their final properties. The particularity of this process is that the critical size of the nucleus decreases with an increase in supercooling of the melt. Crystallization at high supercooling of the melt i.e. in the order of several tens of degrees, allows the development of increasingly smaller nuclei of supercritical size compared to crystallization at low supercooling. The aPLA (T_a=80°C; t_a=3h) sample responds to this crystallization scheme with a high supercooling of the melt exhibiting $(T_m^0 - T_a) > 70°C$. An extremely high nucleation density in low crystallization PLA materials around 80°C has been highlighted [36, 52, 53]. The increase of the crystallization rate in the case of aPLA (T_a=80°C; t_a) samples, shown in Fig. 11a, can thus be attributed to self-nucleation.

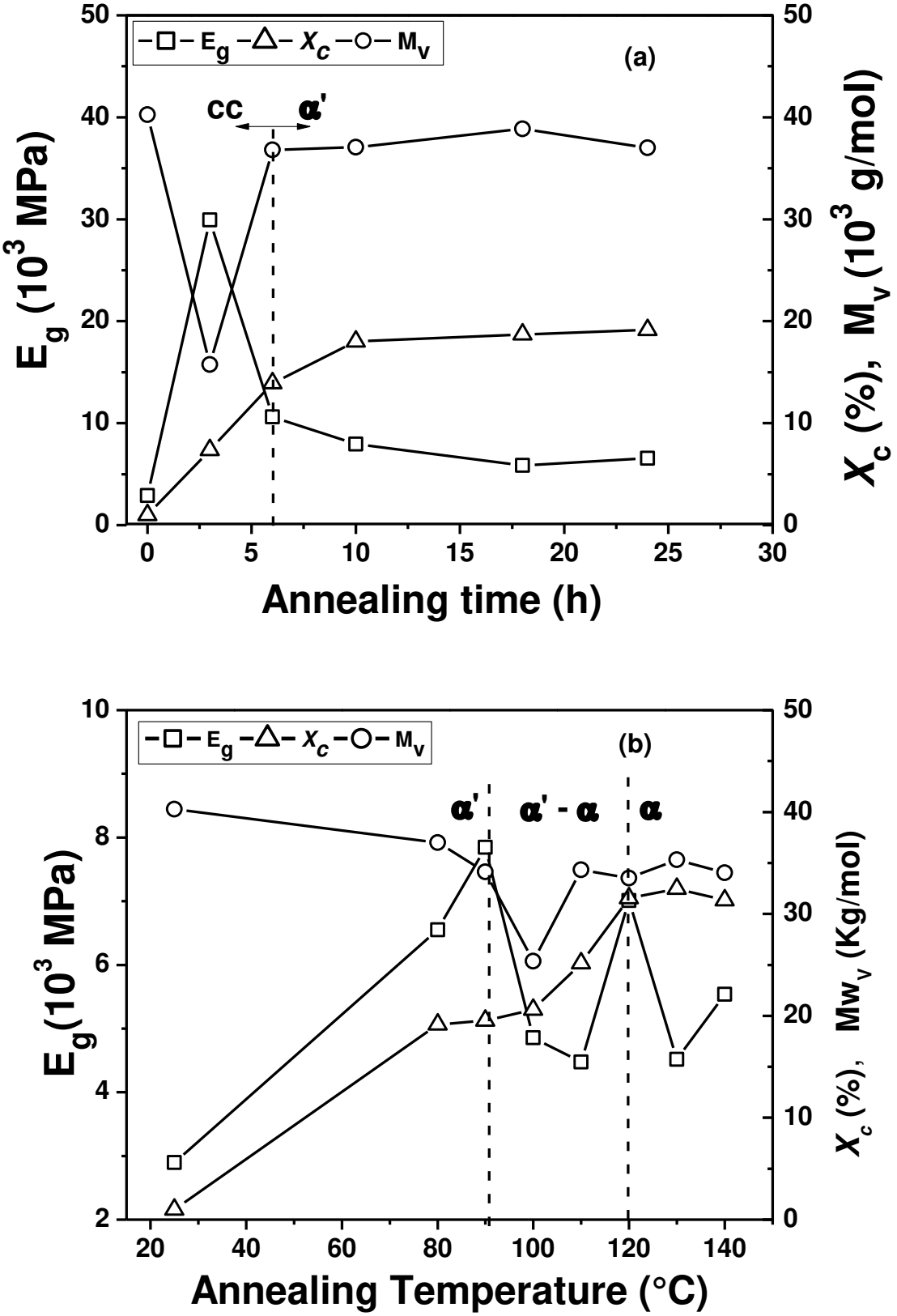

Fig. 11 Glass modulus E_g, crystallinity X_c, and molecular weight M_v, as functions of (a) the times t_a for T_a=80°C; (b) the temperatures T_a for t_a=24 h.

The multitude of spherulites of nanometric dimensions resulting from strong nucleation are considered as crosslinking nodes, thus significantly increasing the material's rigidity. This explains the strong growth of E_g for aPLA (T_a=80°C; t_a=3h). A decrease of E_g was observed for t_a=6 h, beyond which it stabilizes around an average value of 8 000 MPa. This proves that crystallinity strongly depends on t_a and that a critical time exists, corresponding to a critical size of the nucleus, followed by another growth domain of larger crystals [47-53]. The increase of E_g also results from cold crystallinity observed on the thermograms of the samples annealed at 3h and 6h, given by DSC (Fig. 2) and DMA (Fig. 8b). Above t_a=10 h cold crystallinity disappeared, and the fall of moduli, caused by the heat treatment, was damped by the increase of crystallinity (19%). Beyond t_a=10 h, the different properties, E_g, M_v, and X_c, tend towards plateau values around 6 500 MPa, 37 500 g/mol and 19%, respectively. The sudden increase of molecular weight beyond t_a=6 h can be attributed to the crystallinity effect where larger-sized crystallites greatly limit chain mobility and prevent polymer degradation. Another interesting effect is the improvement of the thermo-mechanical properties of aPLA (T_a; t_a) samples around T_a=110°C (i.e. around α'-α phase separation), in particular for the aPLA (T_a: 100-120°C; t_a=24h) sample. Fig. 11b illustrates the evolution of E_g, M_v, and X_c, as function of T_a at t_a=24h. Between 80°C and 90°C, the crystallinity (~19%) was sufficient to increase E_g (from 6 500 MPa to 7 800 MPa) despite the drop of M_v (from 37 000 g/mol to 34 000 g/mol). Between 90°C and 100°C, the strong decrease of M_v (from 34 000 g/mol to 25 000 g/mol) causes a strong drop of E_g (from 7 800 MPa to 4 800 MPa), despite a slight increase of crystallinity. From 100°C to 120°C, the strong increase of crystallinity (from 20% to 31.5%) directly led to an improvement of E_g (from 4 800 MPa to 7 800 MPa), and an increase of M_v from 25 000 g/mol to 35 000 g/mol before stabilizing around 34 000g/mol. This can be explained by the formation of large crystallites hindering chain mobility and, therefore, dramatically reduces the drop in molecular weight. The material exhibits optimal conditions around 120°C in

terms of crystallinity (X_c=31.5%), molecular weight (M_v=35 000 g/mol) and rigidity (E_g=7 800 MPa), thus very favorable conditions for the production of semi-crystalline materials.

Polymorphism in aPLA (T_a=80°C; t_a) and aPLA (T_a; t_a=24h) samples

In terms of polymorphism, two domains can emerge for aPLA (T_a=80°C; t_a: 3-24h) (Fig. 11a): the domain of self-nucleation below t_a=6h with a very high rigidity particularly at t_a=3h, and the domain of α' -crystals corresponding to the appearance of the T_{exo} peak beyond t_a=6 h as described by the DSC thermograms in Fig. 2. The α'-α transition region, showing an improvement of the glass modulus, is not accessible during 24h, limited by the thermal stability of the material. For aPLA (T_a: 80-140°C; t_a=24h) (Fig. 11b), the annealing temperature scan (T_a: 100-120°C) shows a strong increase of the crucial parameters E_g, X_c and M_v, thus predicting the same effects (improvement of rigidity) as the α'-α phase separation in the range T_a: 90-110°C, determined by T_m's peaks (DSC, Fig. 6). Below 90°C, the increase of modulus is mainly due to the extremely high nucleation density in PLA materials, what may be associated with the α' phase. For T_a:90-110°C, a drop of the modulus was observed due to the decrease of M_v despite the strong crystallinity. Between 110°C and 120°C the strong increase in crystallites induces a marked improvement of the modulus, limiting the movement of the chains and improving the mechanical properties of the polymer. Beyond 120°C, crystallinity and molecular weight stabilize, corresponding to the α phase.

Conclusion

In the present report, the thermal behavior of various PLA samples annealed at various T_a and t_a's, were investigated by DSC and DMA measurements. It has been found that the small exothermic peak in the DSC curve just prior to the melting peak, associated with the (α'-α) phase transition, was detected at T_a=80°C and t_a≥10h. This phase separation,

reported by the double T_m melting peak in the range T_a: 90-110°C, can be correlated with the increase of crystallinity for T_a: 100-120°C. DMA data show a sharp enlargement with a decrease of $tan\delta$ peaks of aPLA due to the increase in crystallinity, showing the semi-crystalline behavior of these samples. The salient fact of this work is the substantial growth (~30 000 MPa) of the glassy modulus at T_a=80°C for t_a:3-6 h, due to strong nucleation. The second interesting effect is the improvement of E_g for T_a: 100-120°C, regardless of time t_a, which can be correlated to the increase of crystallinity in the range of T_a: 100-120°C, and the α'-α phase transition (T_a: 90-110°C).

References

1. Lim LT, Auras R, Rubino M (2008) Processing technologies for poly(lactic acid). Prog Polym Sci 33:820-852. http://dx.doi.org/10.1016/j.progpolymsci.2008.05.004
2. Williams CK, Hillmyer MA (2008) Polymers from Renewable Resources: A Perspective for a Special Issue of Polymer Reviews. Polym Rev 48:1-10. http://dx.doi.org/10.1080/15583720701834133
3. Babu RP, O'Connor K, Seeram R (2013) Current progress on bio-based polymers and their future trends. Prog Biomater 2:8. https://doi.org/10.1186/2194-0517-2-8
4. Auras R, Harte B, Selke S (2004) An Overview of Polylactides as Packaging Materials. Macromol Biosci 4:835-864. https://doi.org/10.1002/mabi.200400043
5. Kulinski Z, Piorkowska E (2005) Crystallization, structure, and properties of plasticized poly(L-lactide). Polymer 46:10290-10300. https://doi.org/10.1016/j.polymer.2005.07.101
6. Satti SM, Shah AA, Marsh TL, Auras R (2018) Biodegradation of poly (lactic acid) in soil microcosms at ambient temperature: evaluation of natural attenuation, bio-augmentation and bio-stimulation. J Polym Environ 26:3848-3857. https://doi.org/10.1007/s10924-018-1264-x
7. Chow WS, Teoh EL, Karger-Kocsis J (2018) Flame retarded poly(lactic acid): A review. Express Polym Lett 12:396-417. https://doi.org/10.3144/expresspolymlett.2018.34
8. Cartier L, Okihara T, Ikada Y, Tsuji H, Puiggali J, Lotz B (2000) Epitaxial crystallization and crystalline polymorphism of polylactides. Polymer 41: 8909-8919. https://doi.org/10.1016/S0032-3861(00)00234-2

9. Puiggali J, Ikada Y, Tsuji H, Cartier L, Okihara T, Lotz B (2000) The frustrated structure of poly(L-lactide). Polymer 41: 8921-8930. https://doi.org/10.1016/S0032-3861(00)00235-4
10. Dartora PC, da Rosa Loureiro M, de Camargo Forte MM (2018) Crystallization kinetics and morphology of poly(lactic acid) with polysaccharide as nucleating agent. J Therm Anal Calorim 134:1705-13. https://doi.org/10.1007/s10973-018-7744-3
11. Tábi T, Hajba S, Kovács JG. (2019) The application of the synergistic effect between the crystal structure of poly(lactic acid) (PLA) and the presence of ethylene vinyl acetate copolymer (EVA) to produce highly ductile PLA/EVA blends. J Therm Anal Calorim 138:1287–97. https://doi.org/10.1007/s10973-019-08184-x
12. Simmons H, Tiwary P, Colwell JE, Kontopoulou M (2019) Improvements in the crystallinity and mechanical properties of PLA by nucleation and annealing. Polym Degrad Stab 166:248-257. https://doi.org/10.1016/j.polymdegradstab.2019.06.001
13. Deng L, Xu C, Wang X, Wang Z (2018) Supertoughened Polylactide Binary Blend with High Heat Deflection Temperature Achieved by Thermal Annealing above the Glass Transition Temperature. Chem Eng 28:480–490. https://doi.org/10.1021/acssuschemeng.7b02751
14. Chen J, Deng C, Hong R, Fu Q, Zhang J (2020) Effect of thermal annealing on crystal structure and properties of PLLA/PCL blend. J Polym Res 27:1–11. https://doi.org/10.1007/s10965-020-02206-1
15. Silva Barbosa Ferreira E, Luna CBB, Siqueira DD, Araújo EM, Campos de França D, Ramo Wellen RM (2022) Annealing Effect on Pla/Eva Blends Performance. J Polym Environ 30:541–554. https://doi.org/10.1007/s10924-021-02220-4

16. Agrawal P, Araujo AP, Lima JC, Cavalcanti SN, Freitas DM, Farias GM, Ueki MM, Melo TJ (2019) Rheology, mechanical properties and morphology of poly (lactic acid)/ethylene vinyl acetate blends. J Polym Environ 27:1439-1448. https://doi.org/10.1007/s10924-019-01445-8
17. Barletta M, Puopolo M (2019) Thermo‑Mechanical Properties of Injection Molded Components Manufactured by Engineered Biodegradable. J Polym Environ 27: 2105-2118. https://doi.org/10.1007/s10924-019-01500-4
18. De Santis P, Kovacs A (1968) Molecular conformation of poly(S-lactic acid). Biopolymers 6:299-306. https://doi.org/10.1002/bip.1968.360060305
19. Hoogsten W, Postema AR, Pennings AJ, Ten Brinke G, Zugenmaier P (1990) Crystal structure, conformation and morphology of solution-spun poly(L-lactide) fibers. Macromolecules 23:634-664. https://doi.org/10.1021/ma00204a041
20. Cartier L, Okihara T, Ikada Y, Tsuji H, Puiggali J, Lotz B (2000) Epitaxial crystallization and crystalline polymorphism of polylactides. Polymer 41: 8909-8919. https://doi.org/10.1016/S0032-3861(00)00234-2
21. Puiggali J, Ikada Y, Tsuji H, Cartier L, Okihara T, Lotz B (2000) The frustrated structure of poly (L-lactide). Polymer 41: 8921-8930. https://doi.org/10.1016/S0032-3861(00)00235-4
22. Kalb B, Pennings AJ (1980) General crystallization behaviour of poly(L-lactic acid) Polymer, 21, 607-612. https://doi.org/10.1016/0032-3861(80)90315-8
23. Pan P, Kai W, Zhu B, Dong T, Inoue Y (2007) Polymorphous crystallization and multiple melting behavior of poly(L-lactide): molecular weight dependence. Macromolecules 40:6898-6905. https://doi.org/10.1021/ma071258d
24. Pan P, Zhu B, Kai W, Dong T, Inoue Y (2008) Polymorphic transition in disordered poly(L-lactide) crystals induced by annealing at elevated temperatures. Macromolecules 41:4296–4304. https://doi.org/10.1021/ma800343g

25. Pan P, Inoue Y (2009) Polymorphism and isomorphism in biodegradable polyesters. Prog Polym Sci 34:605–664. https://doi.org/10.1016/j.progpolymsci.2009.01.003

26. Tábi T, Hajba S, Kovács JG (2016) Effect of crystalline forms (α' and α) of poly(lactic acid) on its mechanical, thermo-mechanical, heat deflection temperature and creep properties. Eur Polym J 82:232-243. https://doi.org/10.1016/j.eurpolymj.2016.07.024

27. Jalali A, Huneault MA, Elkoun S (2016) Effect of thermal history on nucleation and crystallization of poly(lactic acid). J Mater Sci 51:7768-7779. https://doi.org/10.1007/s10853-016-0059-5

28. Di Lorenzo M, Rubino P, Immirzi B, Luijkx R, Hélou M, Androsch R (2015) Influence of chain structure on crystal polymorphism of poly (lactic acid). Part 2. Effect of molecular mass on the crystal growth rate and semicrystalline morphology. Colloid Polym Sci 293:2459-2467. https://doi.org/10.1007/s00396-015-3709-2

29. Aleman C, Lotz B, Puiggalı´ J (2001) Crystal structure of the α-form of poly(L-lactide), Macromolecules 34:4795-4801. https://doi.org/10.1021/ma001630o

30. Sasaki S, Asakura T (2003) Helix distortion and crystal structure of the α form of poly(L-lactide). Macromolecules 36:8385-839. https://doi.org/10.1021/ma0348674

31. Zhang JM, Duan Y, Sato H, Tsuji H, Noda I, Yan S, Ozaki Y (2005) Crystal Modifications and Thermal Behavior of Poly(L-lactic acid) revealed by Infrared Spectroscopy. Macromolecules, 38:8012-8021. https://doi.org/10.1021/ma051232r

32. Zhang JM, Tashiro K, Tsuji H, Domb AJ (2008) Disorder-to-Order Phase Transition and Multiple Melting Behavior of Poly(L-lactide) Investigated by Simultaneous Measurements of WAXD and DSC. Macromolecules 41:1352-1357. https://doi.org/10.1021/ma0706071

33. Kawai T, Rahman N, Matsuba G, Nishida K, Kanaya T, Nakano M, Okamoto H, Kawada J, Usuki A, Honma N, Nakajima K, Matsuda M (2007) Crystallization and melting behavior of poly(L-lactic acid). Macromolecules 40:9463–9469. https://doi.org/10.1021/ma070082c

34. Cocca M, Androsch R, Righetti MC, Malinconico M, Di Lorenzo ML (2014) Conformationally disordered crystals and their influence on material properties: the cases of isotactic Polypropylene, isotactic poly(1-butene), and poly(L-lactic acid). J Mol Struct 1078:114–132. https://doi.org/10.1016/j.molstruc.2014.02.038

35. Ohtani Y, Okumura K, Kawaguchi A (2003) Crystallization Behavior of Amorphous Poly(l-Lactide). J Macromol Sci Part B: Phys 42:875-888. https://doi.org/10.1081/MB-120021612

36. Cho T.-Y, Strobl G (2006) Temperature-dependent variations in the lamellar structure of poly(L-lactide). Polymer 47:1036-1043. https://doi.org/10.1016/j.polymer.2005.12.027

37. Zhao Y, Qiu Z, Yan S, Yang W (2011) Crystallization Behavior of Biodegradable Poly(L-lactide)/Multiwalled Carbon Nanotubes Nanocomposites from the amorphous state. Polym Eng Sci 51:1564-1573. https://doi.org/10.1002/pen.21933

38. Schindler A, Harper D (1979) Polylactide II. Viscosity molecular weight relationships and unperturbed chain dimensions. J. Polym Sci 97:2593-9. https://doi.org/10.1002/pol.1979.170170831

39. Tsuji H, Ikada Y (1996) Blends of isotactic and atactic poly(lactide)s: 2. Molecular-weight effects of atactic component on crystallization and morphology of equimolar blends from the melt. Polymer 37:595–602. https://doi.org/10.1016/0032-3861(96)83146-6

40. Fischer EW, Sterzel HJ, Wegner G. Kollid ZZ (1973) Investigation of the structure of solution grown crystals of lactide copolymers by means of chemical reactions. Polym 251:980–990. https://doi.org/10.1007/BF01498927
41. Hoffman JD, Weeks JJ (1962) Melting Process and the Equilibrium Melting Temperature of Polychlorotrifluoroethylene. Journal of Research of the National Bureau of Standards-A, Physics and Chemistry 66:13-28.
42. Zhou C, Li H, Zhang W, Li J, Huang S, Meng Y, Christiansen JD, Yu D, Wu Z, Jiang S (2016) Direct investigations on strain-induced cold crystallization behavior and structure evolutions in amorphous poly(lactic acid) with SAXS and WAXS measurements. Polymer 90:111-121. https://doi.org/10.1016/j.polymer.2016.03.014
43. Mijovic´ J, Sy JW (2002) Molecular Dynamics during Crystallization of Poly(l-lactic acid) As Studied by Broad-Band Dielectric Relaxation Spectroscopy. Macromolecules 35:63-70. https://doi.org/10.1021/ma0203647
44. Tsuji H, Ikada Y (1995) Properties and morphologies of poly(L-lactide): Annealing condition effects on properties and morphologies of poly(L-lactide). Polymer 36:2709. https://doi.org/10.1016/0032-3861(95)93647-5
45. Park SD, Todo M, Arakawa K, Koganemaru M (2006) Effect of crystallinity and loading-rate on mode I fracture behavior of poly(lactic acid). Polymer 47:1357-1363. https://doi.org/10.1016/j.polymer.2005.12.046
46. Keith HD, Padden FJ (1963) Spherulitic Crystallization from the Melt. II. Influence of Fractionation and Impurity Segregation on the Kinetics of Crystallization. J Appl Phys 35:1286. https://doi.org/10.1063/1.1713607
47. Way JL, Atkinson JR, Nutting J (1974) The effect of spherulite size on the fracture morphology of polypropylene. J Mater Sci 9:293–299. https://doi.org/10.1007/BF00550954

48. Xu Y, Wang Y, Xu T, Zhang J, Liu C, Shen C (2014) Crystallization kinetics and morphology of partially melted poly(lactic acid). Polymer Testing 37:179-185. https://doi.org/10.1016/j.polymertesting.2014.05.012

49. Michell RM, Mugica A, Zubitur M, Müller AJ (2015) Self-nucleation of crystalline phases within homopolymers, polymer blends, copolymers, and nanocomposites. Polym Crystallization I 215-256. https://doi.org/10.1007/12_2015_327

50. Sangroniz L, Cavallo D, Müller AJ (2020) Self-nucleation effects on polymer crystallization macromolecules. Macromolecules 53:4581-4604. https://doi.org/10.1021/acs.macromol.0c00223

51. Fillon B, Wittmann JC, Lotz B, Thierry A (1993) Self -nucleation and recrystallization of isotactic polypropylene (α Phase) investigated by Differential Scanning Calorimetry. J Polym Sci Part B: Polym Phys 31:1383-1393. https://doi.org/10.1002/polb.1993.090311013

52. Lorenzo AT, Arnal M, Sánchez JJ, Müller AJ (2006) AJ Effect of annealing time on the self-nucleation behavior of semicrystalline polymers. J Polym Sci Part B: Polym Phys 44:1738. https://doi.org/10.1002/polb.20832

53. Jiang J. Zhuravlev E, Hu WB, Schick C, Zhou DS (2017) The effect of self-nucleation on isothermal crystallization kinetics of poly(butylene succinate) (PBS) investigated by differential fast scanning calorimetry. Chin J Polym Sci 35:1009−1019. https://doi.org/10.1007/s10118-017-1942-5

54. Di Lorenzo ML, Rubino P, Luijkx R, Hélou M (2014) Influence of chain structure on crystal polymorphism of poly(lactic acid). Part 1: effect of optical purity of the monomer. Coll Polym Sci 292:399-409. https://doi.org/10.1007/s00396-013-3081-z

55. Androsch R, Schick C (2015) Crystal nucleation of polymers at high supercooling of the melt. Adv Polym Sci 276:257−288

https://doi.org/10.1002/pi.5707

56. Li X, Su F, Ji Y, Tian N, Lu J, Wang Z, Qi Z, Li L (2013) Influence of the memory effect of a mesomorphic isotactic polypropylene melt on crystallization behavior. Soft Matter 9:8579-8588. https://doi.org/10.1039/C3SM51799C
57. Martinelli A, Calì M, D'llario L, Francolini I, Piozzi A (2011) Effect of the nucleation mechanism on complex poly(L-lactide) nonisothermal crystallization process. Part 1:thermal and structural characterization. J Appl Polym Sci 121:3368-3376. https://doi.org/10.1002/app.33978

Statements and Declarations

Funding

The authors declare that no funds, grants, or other support were received during the preparation of this manuscript.

Competing Interests

The authors have no relevant financial or non-financial interests to disclose.

Author contributions

Assia Zennaki: Investigation, Visualization. **Latifa Zair**: Investigation, Visualization. **Khadidja Arabeche**: Conceptualization, Validation, Data curation. **Lina Benkraled**: Investigation, Visualization. **Abdelkader Berrayah**: Conceptualization, Methodology, Validation, Supervision, Writing- Original draft preparation. **Ulrich Maschke**: Writing-Reviewing and Editing.

Supplementary Files

This is a list of supplementary files associated with this preprint. Click to download.

- SupplementpartMaschkeetal.pdf